INDENTATION AND SCRATCH TESTING – EXPERIMENT AND SIMULATION

F. Pöhl[1], S, Schwarz[2], P. Junker[2], K. Hackl[2], W. Theisen[1]
[1]Lehrstuhl Werkstofftechnik, Ruhr-Universität Bochum, 44801 Bochum, Germany
poehl@wtech.rub.de

[2]Lehrstuhl Materialtheorie, Ruhr-Universität Bochum, 44801 Bochum, Germany

ABSTRACT

Most modern wear resistant materials feature a multiphase microstructure and the macroscopic wear behavior is controlled by the local mechanical properties of the single phases. Indentation testing and in particular nanoindentation allows for the local mechanical characterization of materials and their phases. This paper addresses the determination of important mechanical parameters such as hardness, Young's modulus and indentation energy parameters of single phases in multiphase wear resistant materials. Important influencing factors such as matrix influence on the indentation results of an embedded hard phase, the indentation-size-effect (ISE), the effect of crystallographic orientation, and the fracturing behavior of hard phases are addressed. In addition, the results of scratch tests on the cold work tool steel X210Cr12 and a WC-Co hard metal are presented in order to investigate aspects of the mechanical behavior under abrasion. The deformation behavior under indentation and scratch loading was analyzed by scanning electron microscopy (SEM) and atomic force microscopy (AFM). Besides the experiments supplementary numerical simulations of indentation and scratching testing with the use of the Finite-Element-Method (FEM) are presented.

KEYWORDS

Indentation, scratch testing, deformation behavior, FEM, hard phase

INTRODUCTION

Most abrasion resistant metallic materials are multiphase materials with hard phases embedded in a softer matrix. Due to the small size of the hard phases (e.g. carbides) and their relatively low fracture toughness the mechanical characterization is a complex task and standard characterization methods such as tensile test would fail. Nanoindentation is a suitable method for the local mechanical characterization and has been successfully used for the determination of mechanical parameters of wear resistant materials and their phases [1]. Important mechanical parameters that can directly be calculated from the indentation results are hardness, Young's modulus as well as elastic and plastic indentation energy. Though, several aspects such as matrix influence on the indentation results of an embedded hard phase, the indentation-size-effect (ISE), the effect of crystallographic orientation, or the fracturing behavior of hard phases need to be considered for an accurate measurement and interpretation of the results [2-4]. In this context test related numerical simulations of the indentation process can contribute to the understanding of these aspects and can be used for material development and optimization. Examples of such FEM simulations of nanoindentation are given in [5-8].
With respect to abrasion-resistant metallic materials the local mechanical properties as well as the local deformation behavior of multiphase materials are crucial information for the understanding of the abrasive wear behavior on micro and macro length scale. In addition to nanoindentation tests the abrasive wear behavior can experimentally analyzed by controlled single scratch tests. The tests and their evaluation allow for the quantification of the resistance to scratching and for the determination of the dominating micro-mechanisms of abrasion according to ZUM GAHR [9]. With focus on multiphase materials the influence of phase type, morphology, distribution, and size can be analyzed. In addition to the local mechanical characterization by means of nanoindentation as well as single scratch tests numerical simulations provide supplementary insights into the abrasive

wear behavior. In this context quantities such as phase type, morphology, distribution, and size can systematically be varied and their effect on scratch resistance and resulting stresses and strains can be analyzed. Approaches of numerical simulation of scratch testing can be found in [10-12]. Recent progress in the development of damage models is highly promising in numerically capturing crack initiation and propagation in multiphase materials under mechanical load [13, 14].
This paper addresses the mechanical behavior under indentation and scratch loading considering wear resistant multiphase materials. Firstly, results on important aspects of nanoindentation such as matrix influence on the indentation results of an embedded hard phase, the indentation-size-effect (ISE), the effect of crystallographic orientation, and the fracturing behavior of carbides are presented and discussed. Supplementary FEM simulations are shown in order to give insights into the complex deformation processes. In this context measured mechanical properties of hard phases (carbides) as reinforcement in wear resistant materials are presented.
Secondly, the abrasive wear behavior is studied by the results of scratch tests on multiphase materials. Scratch experiments were performed on the cold work tool steel X210Cr12 as well as a WC-Co hard metal and evaluated in order to reveal the influence of carbides on the scratch behavior and to quantify the dominating micro mechanisms. Results of FEM simulations are presented to give deeper insights into the mechanical behavior of multiphase materials. As an example the crack propagation behavior in a microstructure consisting of hard phases and ductile matrix was numerically investigated and qualitatively compared to the crack propagation in a WC-Co hard metal.

1. MATERIALS AND METHODS

The examined phases and materials including an overview of the conducted experiments are summarized in **Tab. 1**. The sample preparation for nanoindentation and microstructure analysis consisted of grounding with SiC paper followed by successive polishing with diamond suspension with average grain sizes of 6, 3, and 1 µm. Final polishing was performed with oxide polishing suspension with an average grain size of 0.25 µm.

Tab. 1: Summary of investigated materials including the conducted experiments

phase/material	nanoindentation	scratch test	SEM	AFM
VC	✓	-	-	-
TiC	✓	-	-	-
NbC	✓	-	✓	✓
X210Cr12 (M_7C_3)	✓	✓	✓	✓
X210Cr12 (matrix)	✓	✓	✓	✓
WC-Co (12 wt% Co)	-	✓	✓	-
Al_5Fe_2	✓	-	✓	-
X51CrMnN(0.64)20-18	✓	-	✓	-
X2CrNi18-9	✓	-	-	-

Nanoindentation tests were conducted with a CSM indenter (type NHT) equipped with a Berkovich diamond tip. The indentation parameters were an indentation depth of 400 nm with a loading/unloading rate of 50 mN/min as well as a dwell time of ten seconds at maximum load. The hardness and Young's modulus were calculated with the traditional Oliver and Pharr method [15]. In addition, the ratio of elastic to total indentation energy was determined. As apparent in **Fig. 1** the indentation energy is given by the area under the loading and unloading curve. The total indentation energy (W_{pl}) contains the two contributions; the plastic (W_{pl}) and elastic indentation energy (W_{el}). A scratch tester of the company CSM (type NST) was used for scratch tests with a spherical diamond indenter (radius r = 2 µm). A normal load of 20 mN and 60 mN with a scratch speed of 50 µm/min was applied in the case of the X210Cr12 and a progressive scratch with increasing normal load from 3 mN to 800 mN with a loading rate of 200 mN/min in the case of the WC-Co hard metal.

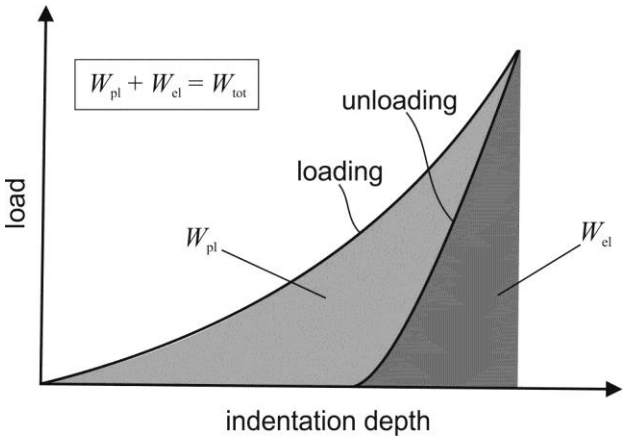

Fig. 1: Schematic illustration of a typical load-displacement curve (P-h curve) with grey-marked elastic and plastic indentation energy

The topography and deformation of residual indentation imprints and scratch grooves were analyzed by atomic force microscopy (AFM) with an AFM in the contact mode (Bruker, type nanos). The scanning speed was varied between 10 and 40 µm/s. The software Image Plus 2.9 was used for data evaluation and three-dimensional visualization.
Scanning electron microscopy (Tescan, type Mira3) was used to analyze the microstructure, phase morphology, residual imprints, and scratch grooves. Addionally, in-situ indentation experiments were conducted with an SEM indentation module of the company Nanomechanics (type NanoFlip).
FEM simulations were performed using the FEM software ABAQUS (version 6.11). Indentation testing was simulated with a conical rigid tip with an included half-apex angle θ of 70.3° indenting an elasto-plastic material or phase, respectively. A conical indenter with a half-apex angle of 70.3° leads to the same area-to-depth function as that of a Berkovich indenter. Numerous studies have shown that this approach sufficiently captures the response of a full-3D model [16]. Details concerning the FEM modeling are given in [2, 17].
Scratch testing was simulated with a 3d model and an irregular rigid abrasive grain scratching an elasto-plastic material including damage. Analogous models are described in [18]. The material model used for the simulations presented in **Figs.** 20 a) and b) can be found in [13, 14]. It is based on two scalar quantities: firstly, the HELMHOLTZ free energy which depends on the elastic strain and a damage parameter has to be specified and furthermore an approach for the dissipation which depends on the rates of microstructural change has to be formulated. Here, the rates of the damage parameter and the plastic strains enter the dissipation. For the well-known problem of mesh dependent finite element results the material model makes use of a rather simple but extremely effective strategy for regularization which can also be found in more detail in [13, 14].

2. RESULTS AND DISCUSSION

Local mechanical characterization of multiphase materials be means of nanoindentation

The macroscopic mechanical behavior of multiphase materials is controlled by the mechanical properties of the single phases and, thus, there is a great interest in measuring their local mechanical properties. Though, the mechanical characterization of single phases in the order of microns or nm is a complex task and standard characterization methods such as tensile test would fail. This is in particular the case when macroscopic brittle phases (e.g. carbides) are to be examined. A proven method for local mechanical characterization of single phases is Nanoindentation. **Fig. 2** shows the local indentation process with the indenter being in contact with the surface, with a maximum load of 50 mN applied to the indenter, and after unloading. Through the measurement of the load-displacement curve (P-h curve) and its analysis (Oliver and Pharr method) important mechanical parameters such as hardness and Young's modulus can directly be determined. Though, several aspects need to be considered for an accurate measurement and interpretation of the results. Firstly, this chapter presents general aspects and phenomenon that

often occur during nanoindentation of small phases and single grains of polycrystalline materials, respectively. Secondly, and with respect to wear resistant metallic materials (abrasion), results of nanoindentation experiments on carbides are shown.

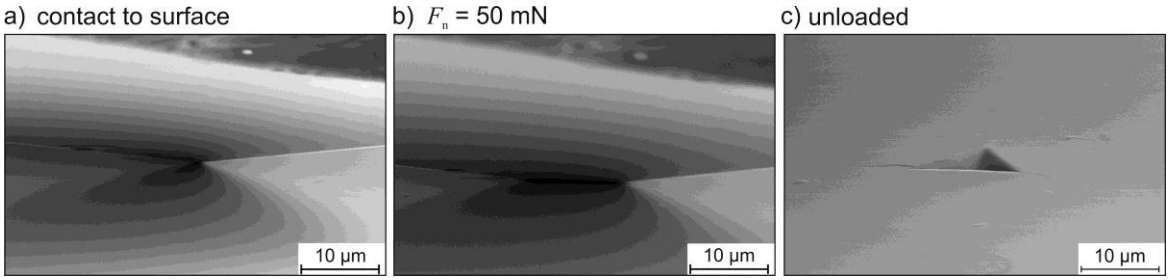

Fig. 2: Illustration of the in-situ indentation process of the phase Al_5Fe_2

Specific aspects of the indentation of single phases and grains of polycrystalline materials which are exemplarily addressed are:

- Influence of the matrix on the indentation results of an embedded hard phase
- Indentation-size-effect (ISE) in metallic and ceramic materials
- Influence of crystallographic orientation on the indentation results
- Fracturing behavior of brittle phases

Fig. 3 shows a residual imprint in NbC carbide embedded in a softer tool steel matrix. FEM simulations of this configuration give an insight into the deformation behavior of the compound and reveal that both carbide and surrounding matrix are plastically deformed. Since the matrix has lower strength the measurement represented by the P-h curve is significantly affected. In this example, the maximum force of the P-h- curve is underestimated by 28 %. As a result, hardness and Young's modulus of the hard phase (both are lower for the steel matrix) are also underestimated. In addition to hard phase size, morphology, and indentation depth the mechanical properties of hard phase and matrix are also critical influencing factors [2]. With the use of test-related FEM simulations the matrix influence can be characterized for given configurations and may reveal affected test data. The slope of the loading curve also gives indications of possible matrix influences since it can be significantly reduced by the matrix.

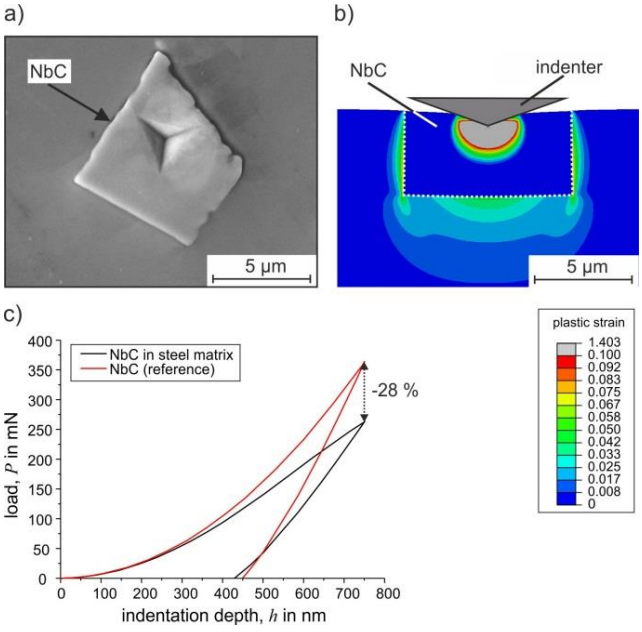

Fig. 3: a) Residual indentation imprint in an NbC embedded in a softer steel matrix b) numerically calculated plastic strain distribution in the NbC and the matrix caused by indentation c) matrix influence on the numerically calculated P-h curves

Another important phenomenon that can significantly affect the indentation results is the indentation-size-effect (ISE). In the case of self-similar indenters (e.g. Berkovich indenter) the ISE is expressed by an increase in measured hardness (strength) with decreasing indentation depth and in the case of spherical indenters by an increase in measured hardness with decreasing indenter diameter. The ISE is accounted for the local density of geometrical necessary dislocations (GNDs) induced in the material during indentation. According to the NIX and GAO model the density of GNDs is significantly increasing with decreasing indentation depth of a self-similar indenter (e.g. Berkovich indenter) or with decreasing diameter of a spherical indenter [19]. In addition to the density of the statistical stored dislocations (SSDs) the distinct increase in the density of the GNDs leads to an increase in strength and, thus, an increase in measured hardness. **Fig. 4** a) illustrates the significant increase in hardness with decreasing indentation depth of the highly affected austenitic steel X2CrNi18-9 measured with a Berkovich indenter. FEM results given in Fig. 4 b) proof that the increase in hardness can be explained by an increase in strength. With graded mechanical properties the experimental P-h curve in **Fig. 4** c) can be reproduced in good agreement. The cause of the local higher strength depending on indentation depth is found in the increase in GND density according to NIX and GAO.

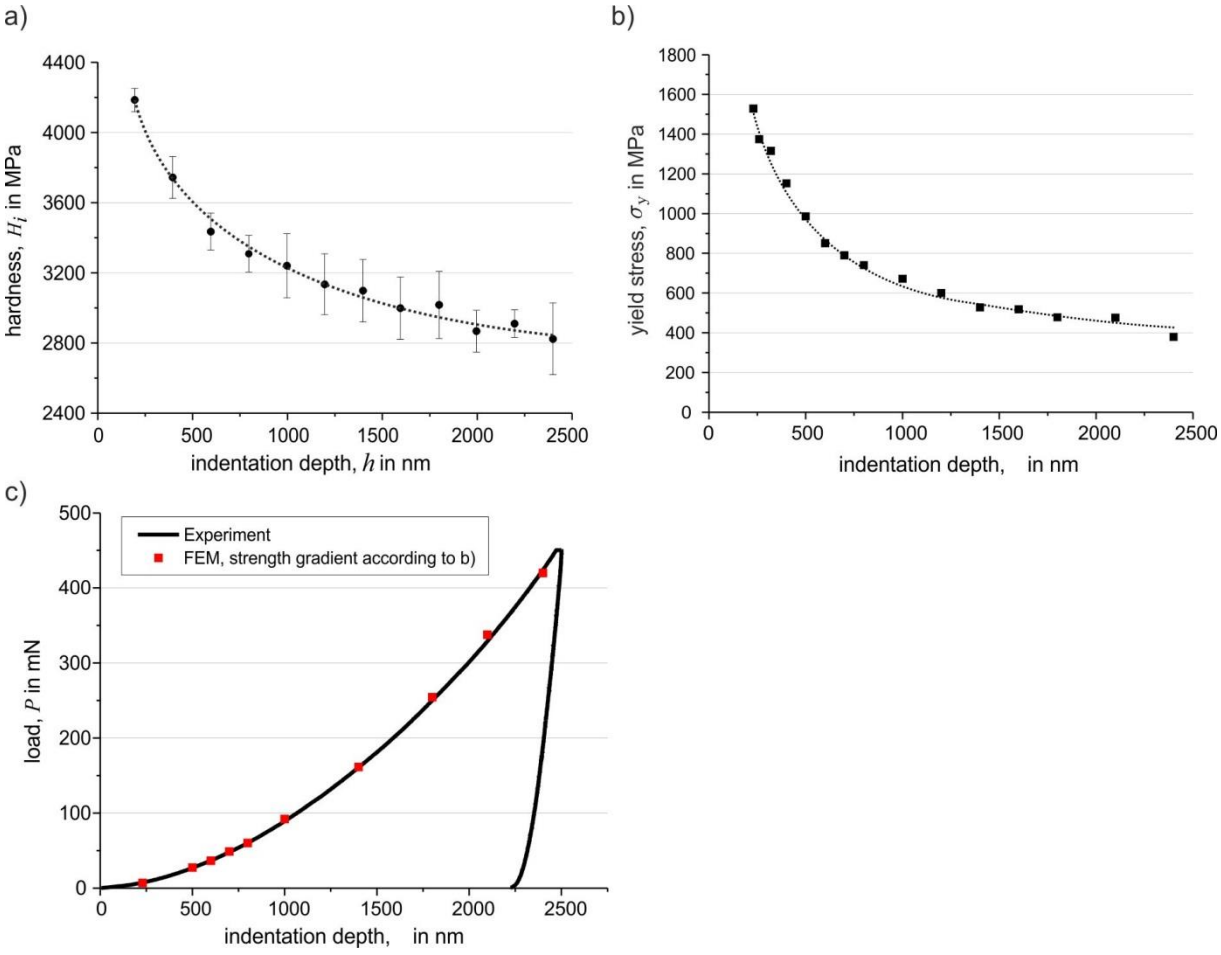

Fig. 4: a) Indentation size effect for the austenitic steel X2CrNi18-9 measured with a Berkovich indenter b) determined depth-dependent flow stress of X2CrNi18-9 c) comparison between the experimental P-h curve of X2CrNi18-9 and the numerically calculated loading curve with the depth-dependent flow stress given in b)

Not only metals, but also ceramic materials can show an ISE [20-23]. **Fig. 5** reveals that monocarbides such as TiC can exhibit an ISE. Compared to e.g. austenitic steels the ISE is less pronounced, even though it is distinctly visible at shallow indentation depths of the Berkovich indenter. Since it is caused by GNDs the results indicate that dislocation movement is a dominant deformation mechanism during indentation of monocarbides. SHINDE et al. and BREVAL also revealed with transmission electron microscopy (TEM) severe dislocation slip caused by

indentation in (TiW)C and TiC carbide at ambient temperature, respectively [24, 25]. In conclusion, caution should be exercised by comparing the hardness of different materials measured at different indentation depths and with different indenter geometries. This applies to metallic materials as well as to hard phases and ceramics such as carbides.

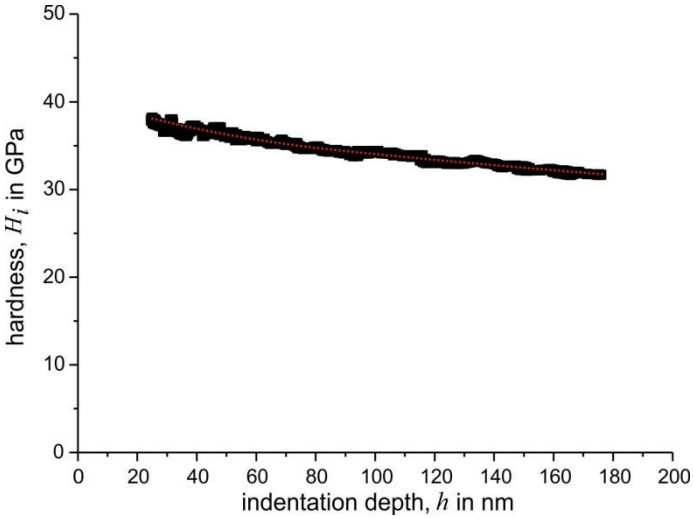

Fig. 5: Indentation-size-effect (ISE) for TiC (Berkovich indenter)

Since crystalline materials are mechanically anisotropic locally derived properties such as hardness are depend on the crystal orientation that is being indented. An example of the anisotropic mechanical behavior is given in **Fig. 6**. The figure shows the grain orientation image of an austenitic stainless steel derived by electron back scatter diffraction (EBSD) technique. A matrix with 256 single indents was established in order to quantify the hardness of the individual grains. From **Fig. 6** it is evident that the hardness is higher for green near (101)-oriented grains in comparison to the blue near (111)-oriented grains. Due to the imposed stress field and the orientation-dependent activation of dislocation gliding plastic deformation is more easily achieved in the (111)-oriented grains. Thus, plastic deformation is facilitated leading to lower hardness values. Mechanically anisotropic behavior is an important influencing factor on the indentation results not only for polycrystalline metals, it is also important for e.g. carbides. HANNINK et al. found significant hardness anisotropy in cubic carbides (TiC, VC, and NbC) which are dependent on the active slip system in the crystal [26].

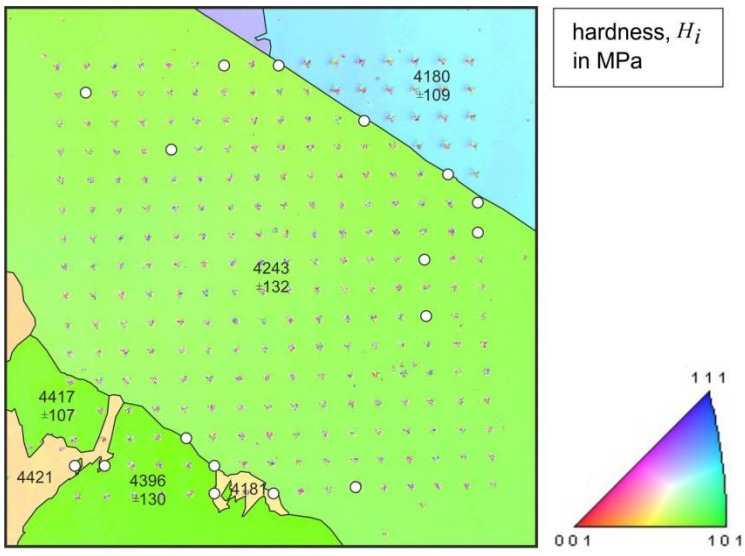

Fig. 6: Crystallographic anisotropic mechanical behavior of X51CrMnN(0.64)20-18 revealed by electron back scatter diffraction (EBSD) and nanoindentation. The average hardness is labelled in the single grains.

The last aspect being shortly addressed is the deformation and fracturing behavior of macroscopic brittle phases under indentation load. The macroscopic behavior of hard phases under ambient temperature and uniaxial loading or bending is usually brittle with no plastic deformation. In contrast, however, the deformation behavior under indentation load especially in small scale testing is relatively ductile. The ductile behavior finds expression in indentation imprints with little or no fracture in the nm regime as apparent in **Fig. 7** a). This is due to the highly hydrostatic stress conditions induced by the indenter. The high hydrostatic component of the stress tensor can mainly inhibit brittle fracture at low loads and leads to the activation of dislocation glide. Though, the limited dislocation movement and interaction between slip bands in hard phases such as carbides in combination with higher indentation loads can result in the formation of cracks [24]. These cracks can be used to estimate the fracture toughness of the phases with empirical equations [4]. **Fig. 7** shows indentation imprints in NbC and the very brittle intermetallic phase Al_5Fe_2. While for the NbC no crack formation is observed the imprint in Al_5Fe_2 has large cracks at the corners. **Fig. 8** illustrates the formed cracks in Al_5Fe_2 under maximum applied load of 50 mN.

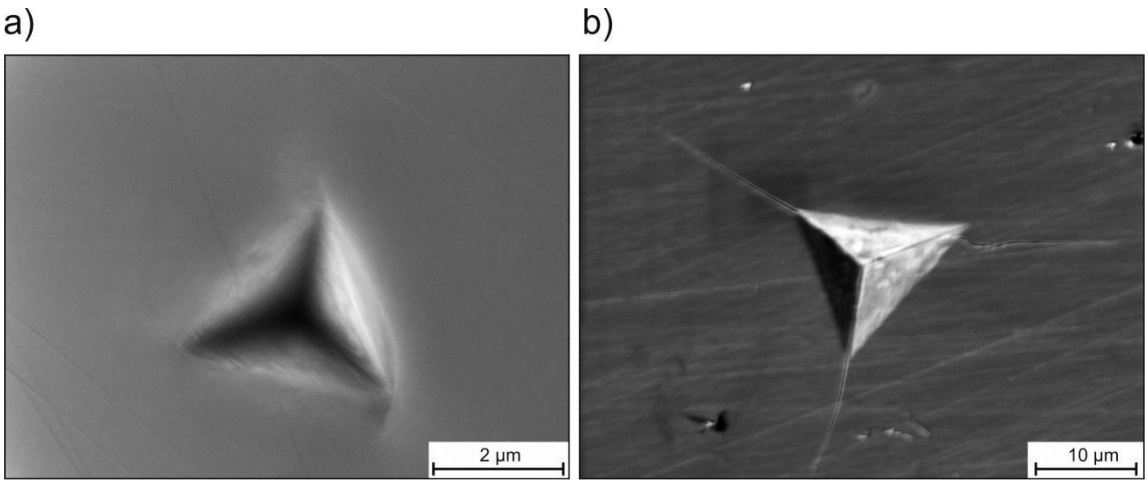

Fig. 7: a) SEM image of an indentation imprint in NbC b) SEM image of an indentation imprint in AL_5Fe_2 with formed cracks at the corners

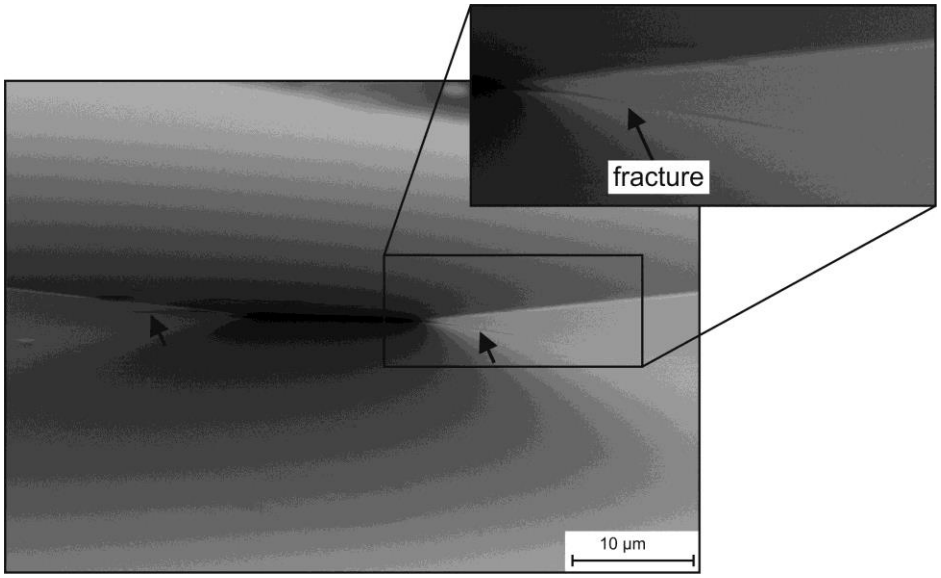

Fig. 8: SEM image of in-situ indentation and crack propagation in Al_5Fe_2

As can be seen in **Fig. 9** higher loads (h_{max} = 750 nm) also lead to crack formation in NbC. The SEM image in a) illustrates the inhomogeneous deformation by deformation bands and crack formation. **Fig. 9** b) shows a 3d image of the crack at the corner of the imprint. Among the analysis of deformation behavior and estimation of fracture toughness the induced cracks can significantly

influence the P-h curve and, thus, measured hardness and Young's modulus by the appearance of pop-in events. Comparison of the two P-h curves in **Fig. 10** reveals that the pop-in event significantly influences the progression of the curve. The forces are shifted to lower forces leading to lower hardness, Young's modulus, and W_{el}/W_{tot} values.

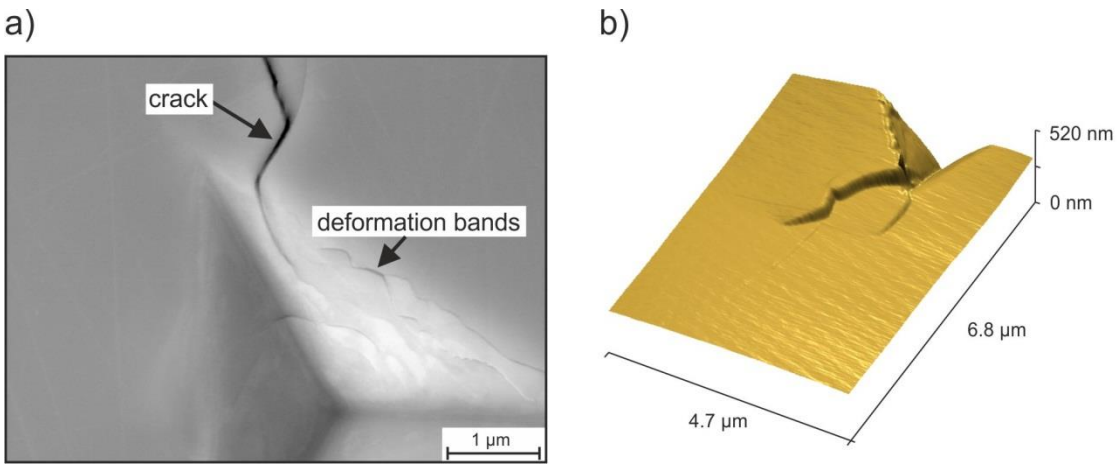

Fig. 9: a) SEM image of indentation imprint in NbC (h_{max} = 750 nm) showing deformation bands and a formed crack b) 3d topography image of a formed crack at the edge of the imprint in NbC

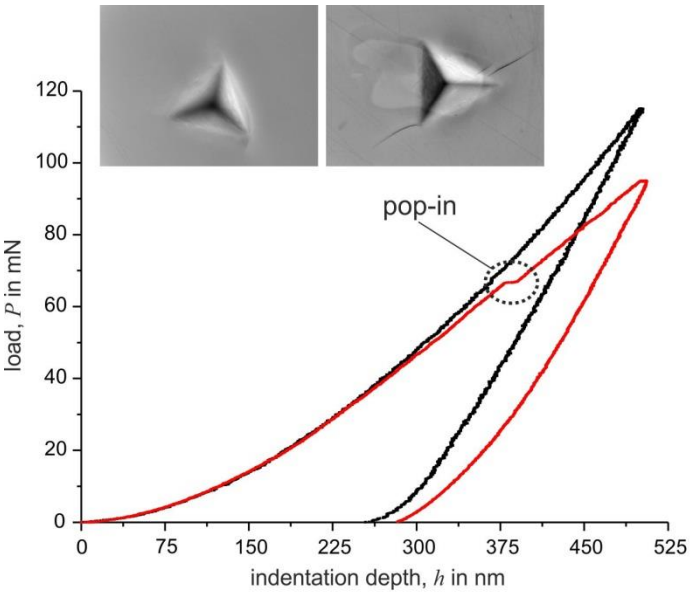

	H_i in GPa	HV	E in GPa	W_{el}/W_{tot} in %
NbC	33.3	3087	357	56
NbC (with pop-in)	23.4	2169	321	43

Fig. 10: Measured P-h curves and parameters for NbC showing the effect of crack formation which finds expression in a pop-in event

With respect to abrasion-resistant metallic materials the mechanical properties as well as the local deformation behavior of hard phases and martensitic steel matrix are considered more closely. Wear resistant steels and in particular tool steels often feature a microstructure consisting of hard phases embedded in martensitic matrix. Carbides such as VC, TiC, NbC or M_7C_3 are frequently used in a high amount as reinforcement particles in abrasion-resistant metallic materials. Due to their high hardness they can effectively act as barriers to attacking abrasive particles. **Tab. 2** summarizes the mechanical parameters of typical hard phases (carbides) and the martensitic steel matrix of the cold work tool steel X210Cr12. Due to the dominant covalent bond the monocarbides VC, TiC, and NbC show the highest hardness with values between 2763 HV and 2964 HV (indentation depth of 400 nm). In comparison the M_7C_3 carbides have a distinct lower hardness of

1773 HV at equal indentation depth. The lowest hardness is observed for the martensitic steel matrix (784 HV). The determined W_{el}/W_{tot} ratios of the phases show the same ranking compared to the hardness with monocarbides having the highest, M_7C_3 a slightly lower, and martensitic matrix the lowest ratio. This also holds true for the ranking of the Young's modulus. **Fig. 11** illustrates typical indentation imprints in the martensitic matrix and M_7C_3 carbide.

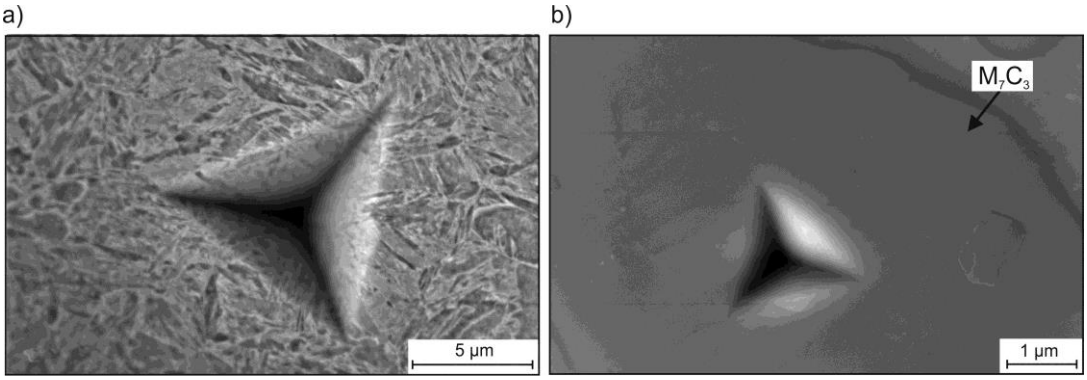

Fig. 11: a) SEM image of an imprint in the martensitic matrix (etched) b) SEM image of an imprint in an M_7C_3 carbide

The measured parameters together with the fracture behavior as exemplarily showed before give insight into the deformation behavior of the single phases. On the one hand this also improves the understanding of the mechanical behavior of multiphase materials and on the other hand the knowledge can be used for the development and optimization of multiphase microstructures for given applications. With this regard numerical simulations are useful tools. An example is given in **Fig. 12**. It shows the results of FEM simulations revealing the influence of volume fraction of spherical monocarbides with 80 HRC embedded in a matrix with 69 HRC on the compound macro Rockwell hardness.

Tab. 3: Mechanical properties of typically used carbides in tool steels and martensitic steel matrix

Phase	Indentation hardness H_i in GPa	Converted Vickers hardness	Young's modulus in GPa	W_{el}/W_{tot} ratio in %
VC [23]	30.7 ± 2.0	2845 ± 182	423 ± 20	50 ± 3
TiC [23]	29.7 ± 2.5	2763 ± 227	392 ± 26	57 ± 5
NbC [23]	32.0 ± 3.8	2964 ± 352	431 ± 36	54 ± 4
M_7C_3	18.9 ± 3.6	1773 ± 332	268 ± 21	44 ± 6
Martensite (q) (X210Cr12)	8.2 ± 0.2	784 ± 14	193 ± 10	30 ± 1

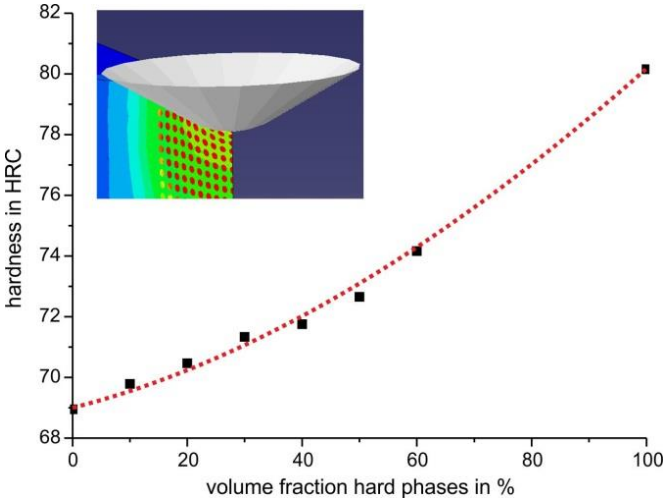

Fig. 12: Numerically calculated relationship between Rockwell hardness and volume fraction of spherical hard phases with hardness 80 HRC embedded in a matrix with 69 HRC

Scratch behavior of multiphase materials

The deformation behavior under abrasion with focus on the acting micro-mechanisms can be characterized with scratch tests under controlled laboratory conditions. Most modern abrasion resistant steels are multiphase materials consisting of higher hard phase amounts embedded in a softer matrix. **Fig. 13** shows the microstructure of the wear resistant cold work tool steel X210Cr12. It consists of chromium-rich M_7C_3 carbides embedded in a martensitic steel matrix. The macroscopic abrasive wear behavior is controlled by the local mechanical properties of the single phases.

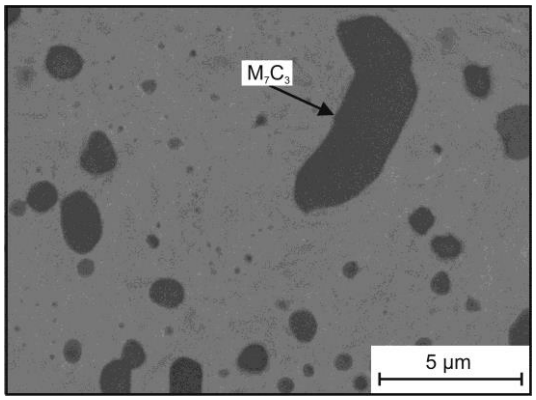

Fig. 13: Microstructure of the cold work tool steel X210Cr12 consisting of martensitic matrix and embedded M_7C_3 carbides

The mechanical properties measured by nanoindentation are given in **Tab. 3**. The high hardness of the carbides strongly improves the abrasive wear resistance. The carbides effectively act as a barrier to attacking abrasive particles. Though, the wear resistance is dependent on morphology, size, and distribution of the carbides and is also dependent on abradant hardness, size, and morphology [27]. The hard carbides are embedded in a martensitic steel matrix with lower hardness which ensures an adequate fracture toughness of the compound system.
Fig. 14 illustrates the deformation behavior of the multiphase material under scratch testing. The constant normal load of the indenter leads to the penetration and scratching of the matrix. The matrix is either flowing to the edges of the scratch (microploughing) or is removed by microcutting. Due to the relatively high toughness of the matrix no microcracking is observed. AFM measurements reveal that microploughing and in particular microcutting are the dominating micro mechanisms (see **Fig. 15**). The f_{ab}-parameter was calculated for four different positions along the scratch in the matrix and calculated to 0.81± 0.04.

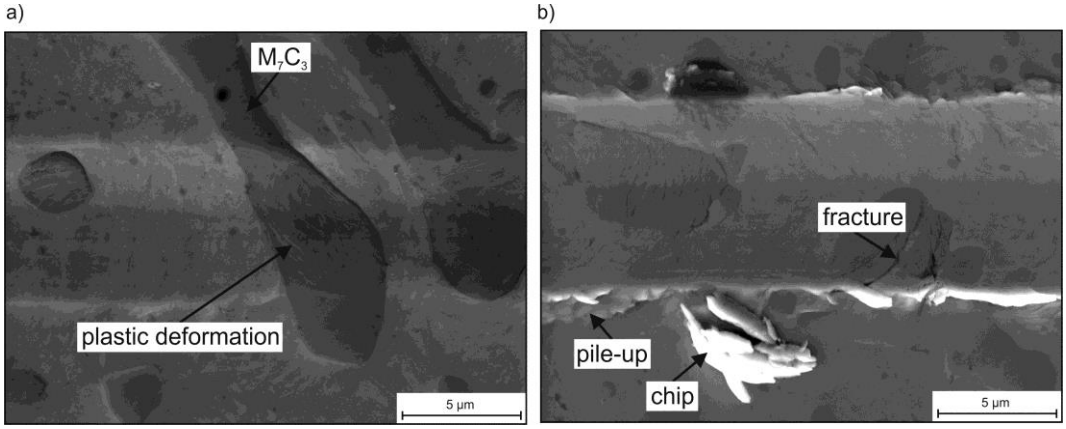

Fig. 14: a) SEM image of a scratch (F_n = 20 mN) in X210Cr12 with microploughing and plastic deformation of M_7C_3 b) SEM image of a scratch (F_n = 60 mN) in X210Cr12 with microploughing, microcutting, and fractured M_7C_3

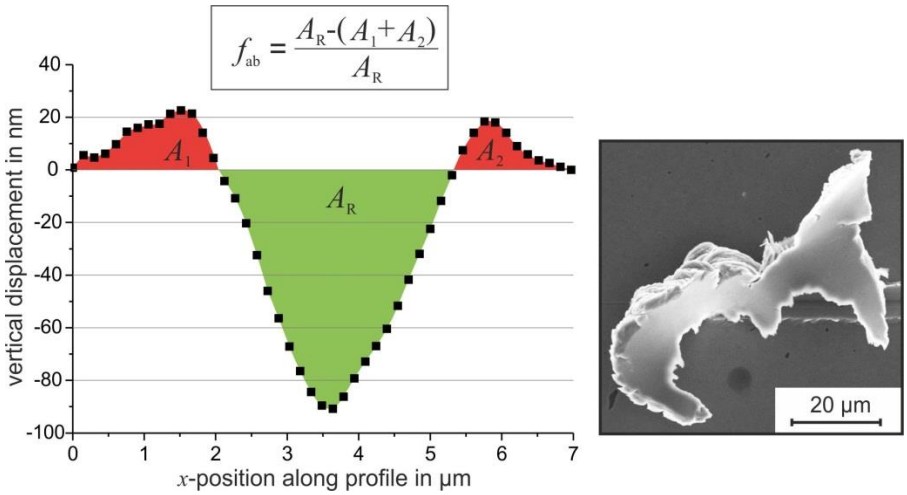

Fig. 15: a) Surface height profile of the scratched martensitic matrix (F_n = 20 mN) and marked areas for the calculation of the f_{ab}-parameter b) Large formed chip by scratching the martensitic matrix

Obtained from **Figs. 16** a) and c) as the indenter enters into contact with large M_7C_3 the penetration depth significantly decreases. At the same time **Figs. 16** b) and d) reveal that the scratch width is also reduced which leads to an overall reduction in material loss and, thus, to an increase in wear resistance. This holds true for carbide sizes larger than the scratch width.

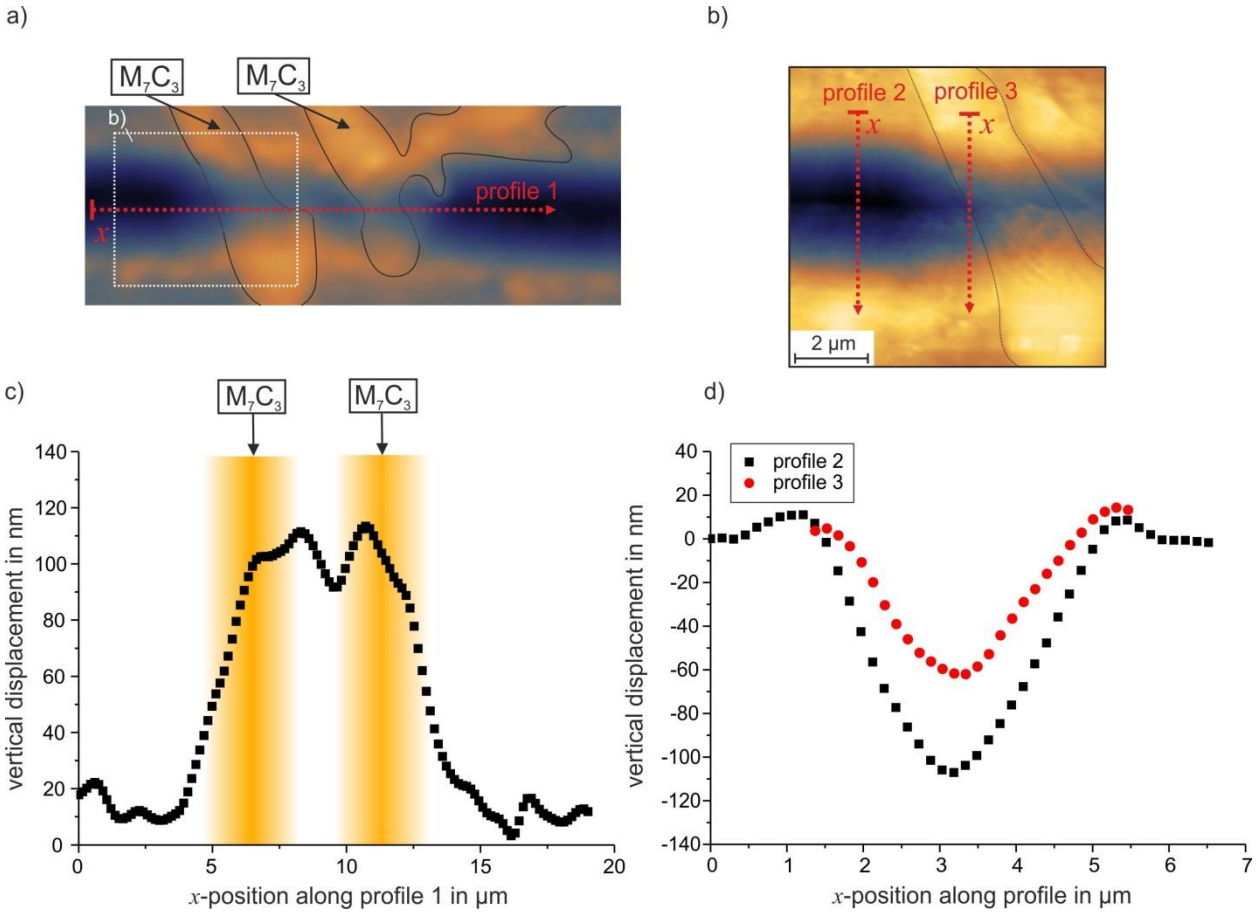

Fig. 16: AFM images and surface profiles of a scratch (F_n = 20 mN) in X210Cr12 (the scratch direction is always from left to right) a) AFM topography image of the scratch b) detail of a) showing the scratch at the transition between matrix and M_7C_3 carbide c) Surface height profile along profile 1 showing the reduction in scratch depth caused M_7C_3 d) Surface height profile along profile 2 and 3 showing the reduction of scratch depth and width caused by M_7C_3

Fig. 17 illustrates the scratch behavior in the case of carbides smaller than the scratch width. It can be seen that the carbide size is too small to be effective. The carbides are pushed into the matrix, ploughed to the sides or chipped out. The local deformation behavior of the carbides is plastic deformation and isolated fracturing (see **Fig. 14**).

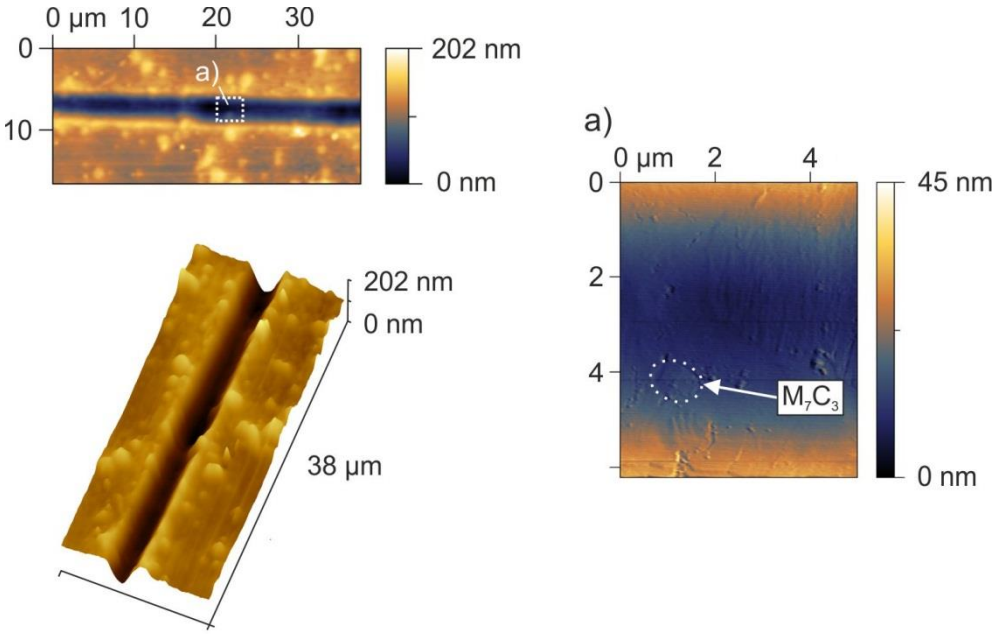

Fig. 17: AFM topography images of a scratch in X210Cr (F_n = 20 mN) with M_7C_3 carbides being smaller than the scratch width

The influence of carbides with different sizes can be analyzed with FEN simulations. As apparent in **Fig. 18** a) small carbides (smaller than the scratch width) are not effective and do not highly increase the wear resistance. They are pushed away or chipped out by the abrasive particle. In contrast, as can be seen in **Fig.18** b) single carbides larger than the scratch width can effectively hinder the abrasive particle from scratching the material. The hard phase cannot be pushed away or chipped out. For a constant load scratch depth and width are both reduced. Such numerical investigations can be established to analyze the influence of hard phase morphology, distribution, or amount on the scratch behavior and, thus, on the abrasive wear behavior. With the use of material parameter determination of hard phases and matrices by nanoindentation different hard phase types and matrices can also be considered. This allows the systematic variation of hard phase type, morphology, distribution, and matrix in order to assist the developing process of materials and microstructures with superior abrasive wear behavior.

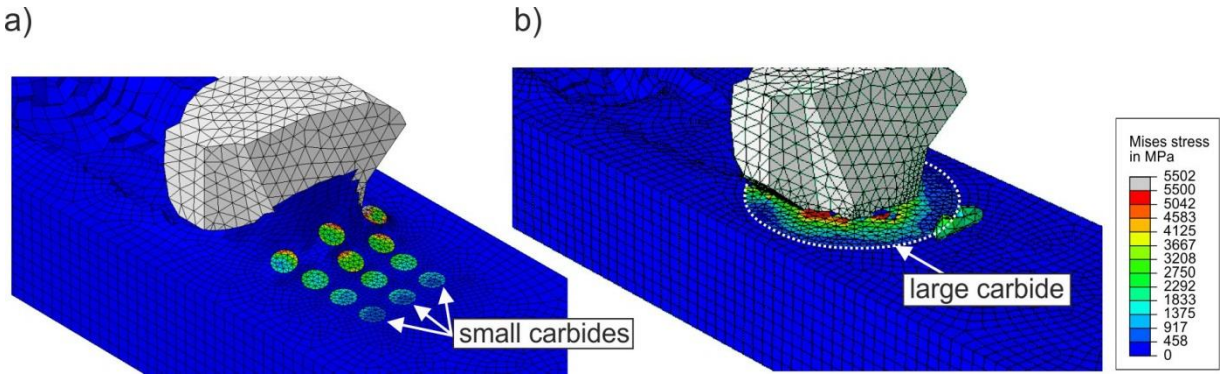

Fig. 18: FEM simulations showing a) the influence of small carbides on the scratch behavior with the abrasive grain being larger than the carbides and b) the influence of carbides being larger than the abrasive grain

Fig. 19 shows the microstructure of a Co-based hard metal with WC. Typical applications are cutting tools used for metal cutting application. In order to achieve a high wear resistance the material consists of a large amount of hard WC. This leads to a very high hardness and compared to tool steels relatively low fracture toughness of the compound. Due to the lower fracture toughness the fracturing and crack propagation behavior is of great relevance. Within the fracture process the Co binder phase plays an important role and has a dominant contribution to the fracture resistance [26].

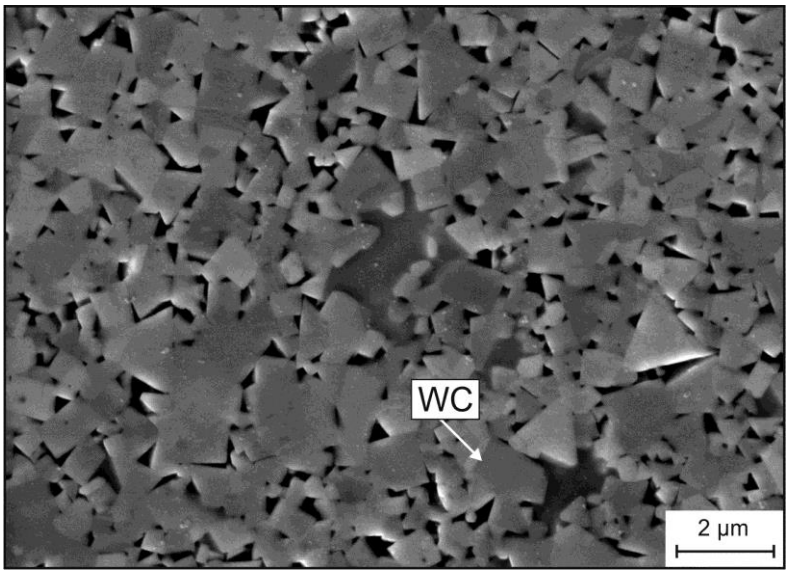

Fig. 19: SEM image of the microstructure of WC-Co hard metal

An induced crack (by Vickers indentation, HV10) is illustrated in **Fig. 20**. The crack propagates mainly along the Co-matrix very closed to the WC-Co interface with isolated WC cleavage. The dominant Co-matrix influence on the fracture behavior indicates that the plastic deformation of the Co-matrix contributes the major portion of the dissipative work during fracture of the compound [26]. Numerical simulations can qualitatively capture the complex fracturing behavior of multiphase materials with carbide phase. **Figs. 20** b) and c) show the numerical simulation of crack propagation in a multiphase material consisting of ductile matrix and embedded blocky hard phases. Analogous to the experiment the effect of secondary hard phase becomes visible. The crack propagates mainly along the ductile matrix. Though, the propagation path is influenced by the hard phases and under unfavorable geometric aspects the hard phase also fractures. From **Fig. 20** it can also be seen that a considerable amount of plastic deformation is occurring in the matrix. Numerical simulations can be established in order to reveal the influence of hard phase morphology, size, or amount on fracture behavior and crack propagation. Furthermore, it can be used for alloy development and microstructure design. The simulations also help to investigate and to better understand the deformation behavior under scratch testing and abrasion load, respectively. As can be seen in **Fig. 21** the deformation during scratching (spherical indenter) changes from elastic to elastic-plastic and elastic-plastic behavior with fracture depending on the applied load. The details in **Figs. 21** a) and b) show fractured particles next to the edges of the scratch. The particles consist of mostly undamaged and partly fractured WC and heavily deformed Co-matrix. Massive cracking is not observed.

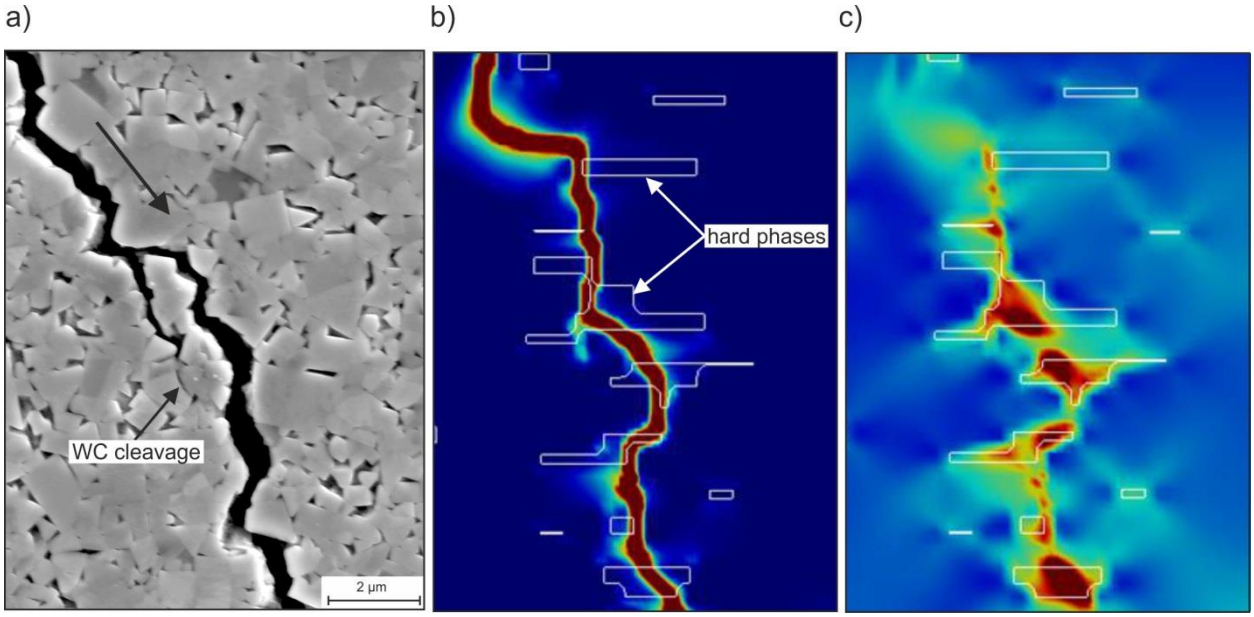

Fig. 20: a) SEM image of formed crack in WC-Co hard metal (the large arrow indicates the propagation direction) b) numerical simulation of crack propagation in multiphase material consisting of matrix and hard phases showing the damage (red color) c) numerical simulation of crack propagation showing the plastic deformation

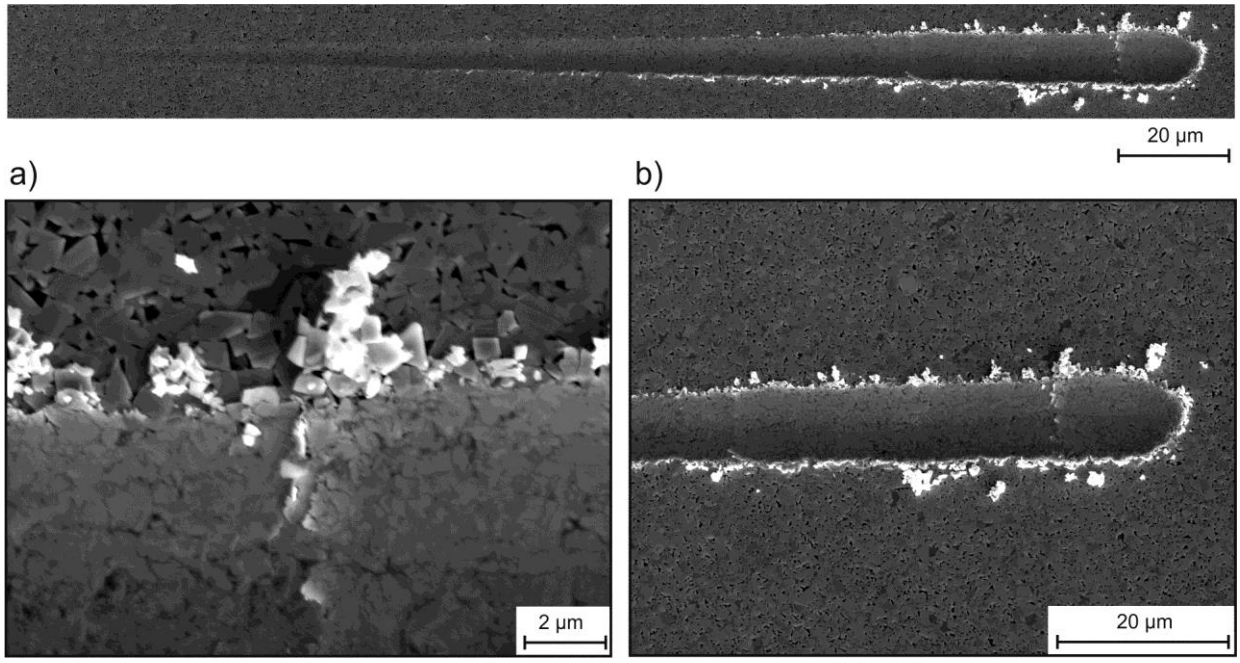

Fig. 21: SEM images of a progressive scratch showing different stages of deformation (F_n progressively increased from 3 mN to 800 mN)

3. CONCLUSIONS

The main conclusions to be drawn are:

- Experimental data and numerical simulations show that the matrix can significantly influence the indentation results of an embedded hard phase. With the use of test-related FEM simulations the matrix influence can be characterized for given configurations and may reveal affected test data.
- In the case of self-similar indenters (e.g. Berkovich indenter) the indentation-size-effect (ISE) is expressed by an increase in measured hardness (strength) with

decreasing indentation depth caused by the local increase in the density of geometrical necessary dislocations. The results show an ISE for the austenitic steel X2CrNi18-9 and also for TiC. Compared to e.g. austenitic steels the ISE is less pronounced, even though it is distinctly visible at shallow indentation depths of the Berkovich indenter.

- Mechanically anisotropic behavior caused by crystallographic grain orientation was revealed by nanoindentation in combination with electron back scatter diffraction (EBSD) technique for the austenitic steel X51CrMnN(0.64)20-18.
- Nanoindentation technique can also be used for the analysis of the fracture behavior of hard phases. The deformation behavior is expressed in discontinuous deformation bands and formed cracks. Cracking may cause pop-in events which leads to an underestimation of hardness and Young's modulus.
- In combination, single phase mechanical properties and numerical simulations are useful for revealing the influence of the microstructure on the macroscopic mechanical behavior. As an example it was shown the results of FEM simulations revealing the influence of volume fraction of spherical monocarbides with 80 HRC embedded in a matrix with 69 HRC on the compound macro Rockwell hardness.
- The scratch behavior of X210Cr12 shows that the matrix is either flowing to the edges of the scratch (microploughing) or is removed by microcutting. Due to the relatively high toughness of the matrix no microcracking is observed. AFM measurements reveal that microploughing and in particular microcutting are the dominating micro mechanisms. As the indenter enters into contact with large M_7C_3 the penetration depth significantly decreases (constant load). At the same time the scratch width is also reduced which leads to an overall reduction in material loss and, thus, to an increase in wear resistance. This holds true for carbide sizes larger than the scratch width.
- Numerical simulations of scratch testing allow the systematic variation of hard phase type, morphology, distribution, and matrix in order to assist the developing process of materials and microstructures with superior abrasive wear behavior.
- Numerical simulations were conducted in order to better understand the fracture behavior of WC-Co hard metal. Analogous to the experiment the effect of secondary hard phase becomes visible. The crack propagates mainly along the ductile matrix. Though, the propagation path is influenced by the hard phases and under unfavorable geometric aspects the hard phase also fractures. It could be seen that a considerable amount of plastic deformation is occurring in the matrix. Numerical simulations can be established in order to reveal the influence of hard phase morphology, size, or amount on fracture behavior and crack propagation. Furthermore, it can be used for alloy development and microstructure design. The simulations also help to investigate and to better understand the deformation behavior under scratch testing and abrasion load, respectively.

REFERENCES

[1] Hill, H, Weber, S, Huth, S, Niederhofer, P., Theisen, W, 2011, The impact of processing on microstructure, single-phase properties and wear resistance of MMCs, Wear, 271, 9-10, pp. 1895-1902

[2] Pöhl, F, Huth, S, Theisen, W, 2014, Finite element method-assisted acquisition of the matrix influence on the indentation results of an embedded hard phase, Materials Science and Engineering: A, 559, 2013, pp. 822-828

[3] Wang, Y, Raabe, D, Klüber, C, Roters, F, 2004, Orientation dependence of nanoindentation pile-up patterns and of nanoindentation microtextures in copper single crystals, Acta Materilia

[4] Feng, Y, Zhang, T, 2014, Determination of fracture toughness of brittle materials by indentation, Acta Mechanica Solida Sinica, 28, 3, pp. 221-234

[5] Dao, M, Chollacoop, N, van Fliet, KJ, Venkatesh, TA, Suresh, S, 2001, Computational modeling of the forward and reverse problems in instrumented sharp indentation, Acta Materialia, 49, pp. 3899-3918

[6] Sun, Y, Bell, T, Zheng, S, 1995, Finite element analysis of the critical ratio of coating thickness to indentation depth for coating property measurements by nanoindentation, Thin Solid Films, 258, pp. 198-204

[7] Taljat, B, Pharr, GM, 2004, Development of pile-up during spherical indentation of elastic-plastic solids, International Journal of Solids and Structures, 41, 14, pp. 3891-3904

[8] Rosenberger, MR, Forlerer, E, Schvezov, CE, 2007, Modeling the micro-indentation of metal matrix composites, Materials Science and Engineering A, 463, pp. 275-283

[9] Zum Gahr, KH, 1983, Furchungsverschleiß in: Reibung und Verschleiß Mechanismen – Prüftechnik – Werkstoffeigenschaften, Ed. Zum Gahr, KH, DGM, Oberursel, pp. 135-156

[10] Holmberg, K, Laukkanen, A, Ronkainen, H, Wallin, K, Varjus, S, Koskinen, J, 2006, Tribological contact analysis of a rigid ball sliding on a hard coated surface Part I: Modeling stresses and strains, Surface & Coatings Technology, 200, pp. 3793-3809

[11] Prasad, A, Dao, M, Suresh, S, 2009, Steady-state frictional sliding contact on surfaces of plastically graded materials, Acta Materialia, 57, pp. 511-524

[12] Wredenberg, F, Larsson, PL, 2010, On the stress distribution at scratching of thin film structures, Coatings Technology and Research, 7, 5, pp. 623-635

[13] Junker, P, Schwarz, S, Makowski, J, Hackl, K, 2015, A gradient-based regularization approach without field functions, Continuum Mechanics and Thermodynamics, under review.

[14] Schwarz, S, Junker, P, Hackl, K, 2015, A regularization approach for damage models based on a displacement gradient, Proc. Appl. Math. Mech. 15, 151 – 152

[15] Oliver, WC, Pharr, GM, 1992, An improved technique for determining hardness and elastic modulus using load and displacement sensing indentation experiments, Materials Research, 7, 6, pp. 1564-1583

[16] Cai, X, 1992, Finite-element method for simulation of elasto-plastic indentations by various indentors, Materials Science Letters, 11, pp. 1527-1531

[17] Pöhl, F, Huth, S, Theisen, W, 2014, Indentation of self-similar indenters: An FEM-assisted energy-based analysis, Journal of the Mechanics and Physics of Solids, 66, pp. 32-41

[18] Wielage, B, Lampke, T, Müller, L, Weber, D, 2008, Verifizierung numerischer Verfahren zur Modellierung abrasiver Verschleißprozesse durch die Berechnung von Scratchtests, Materialwissenschaft und Werkstofftechnik, 39, 12, pp. 963-966

[19] Nix, WD, Gao, H, 1998, Indentation size effects in crystalline materials: A law for strain gradient plasticity, Journal of the Mechanics and Physics of Solids, 46, 3, pp. 411-425

[20] Nino, A, Tanaka, A, Sugiyama, S, Taimatsu, H, 2010, Indentation size effect for the hardness of refractory carbides, Materials Transactions, 51, 9, pp. 1621-1626

[21] Gong, J, Wu, J, Guan, Z, 1999, Analysis of the indentation size effect on the apparent hardness for ceramics, Materials Letters, 38, pp. 197-201

[22] Peng, Z, Gong, J, Miao, H, 2004, On the description of indentation size effect in hardness testing for ceramics: Analysis of the nanoindentation data, Journal of the European Ceramic Society, 24, pp. 2193-2201

[23] Pöhl, F, Weddeling, A, Theisen, W, 2015, Mechanical characterization of hard phases by means of nanoindentation, Proceedings of 3rd Symposium on Nb-Mo alloying in steel and iron

[24] Shinde, SL, Jayaram, V, Sinclair, R, 1983, Microstructural characterization of deformation and precipitation in (W,Ti)C, in: Science of hard materials, Ed. Visvanadham, RK, Rowcliff, DJ, Gurland, J, Plenum Press, New York, pp. 137-154

[25] Breval, E, 1981, Microplasticity at room temperature of single-crystal titanium carbide with different stoichiometry, Journal of Materials Science, 16, pp. 2781-2788

[26] Hanning, HJ, Kohlstedt, DL, Murray, MJ, 1972, Slip system determination in cubic carbides by hardness anisotropy, Proceeedings of the Royal Society London A, 326, pp. 409-420

[27] Ed. Berns, H, 1998, Hartlegierungen und Hartverbundwerkstoffe, Gefüge, Eigenschaften, Bearbeitung, Anwendung, Springer, Berlin Heidelberg

[28] Hong, J, Gurland, J, 1983, A study of the fracture process of WC-Co alloys, in: Science of hard materials, Ed. Visvanadham, RK, Rowcliff, DJ, Gurland, J, Plenum Press, New York, pp. 649-666